Article

Photoaging Promotes Toxic Micro/Nanoplastics Release from PLA/PBAT Biodegradable Plastic in Gastrointestinal Condition

Xuri Wu, Han Zhang, Jingwen Chen, Feng Tan,* Rui Cai,* and Yan Wang

Cite This: *Environ. Health* 2025, 3, 446−457

Read Online

ACCESS | 📊 Metrics & More | 📖 Article Recommendations | 🅢🅘 Supporting Information

ABSTRACT: The release of micro/nanoplastics (MNPs) from biodegradable plastics in gastrointestinal environments due to photoaging, along with their associated mechanisms and potential cytotoxicity, is largely unknown. Here, we show that poly(lactic acid)/poly(butylene adipate-*co*-terephthalate) (PLA/PBAT) films undergo ultraviolet photoaging, resulting in increased surface roughness and a higher quantity of MNPs on the surface. This aging process involves the generation of carbon- and oxygen-centered free radicals, chain scission, and the formation of oxidation products with hydroxyl and carbonyl groups. These MNPs can be released under water shear force, significantly increasing the normalized mass loss of aged films to approximately 0.128 mg/cm^2 (18 times higher than that of unaged films in water). In the gastrointestinal environment, the normalized mass loss further increases to about 0.196 mg/cm^2 (28 times higher), likely due to potential enzymatic digestion and ion-swelling effects. These MNPs, primarily composed of PLA, are smaller and carry more negative charges under gastrointestinal conditions. In the THP-1 cell model, these MNPs affect cell viability in a dose-dependent manner. MNPs obtained through ultrafiltration, compared to those collected via centrifugation, display a broader size distribution and induce more pronounced toxicity in THP-1 cells, with an EC$_{50}$ of 243 mg/L. Preliminary comparative analysis indicates that PLA/PBAT-derived MNPs present toxicity risks comparable to, or greater than, those of conventional plastic MNPs. These findings underscore the potential hazards associated with biodegradable plastics.

KEYWORDS: PLA/PBAT biodegradable plastic, UV aging, gastrointestinal digestion, MNPs, cell viability
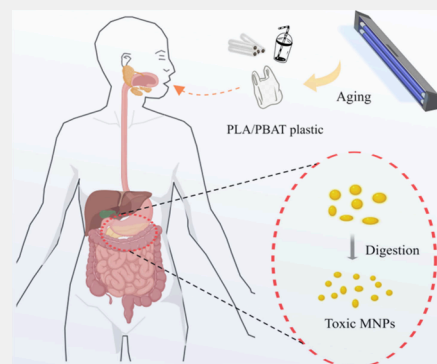
◼ INTRODUCTION

Plastic products, renowned for their exceptional material properties and cost-effectiveness, are pervasive across various sectors. However, due to inadequate recycling, disposal practices, and poor management of plastic waste, the accumulation of plastic in the environment has been relentless. In 2019, global plastic production reached 370 million tons, of which only 9% was recycled, 12% was incinerated, and the remainder ended up in landfills or entered the environment.[1] There, it gradually fragmented into microplastics (<5 mm) and nanoplastics (<100 nm or <1 μm) under various environmental influences, while also degrading into dissolved organic carbon, eventually converting to CO$_2$ through microbial activity.[2−4] The global plastic cycle has led to plastic pollution everywhere.[5] The presence of these plastics in water systems,[6] terrestrial systems,[7] and even the indoor and outdoor air breathed by humans[8] has been documented. It is important to note that multiple studies have shown these MNPs pose potential threats to cells and organisms.[9−11] Plastic has emerged as one of the greatest contemporary threats and most significant challenges of the 21st century for the environment and human wellbeing.

As a consequence, biodegradable plastics have been identified as a promising solution to mitigate plastic waste, with their use becoming increasingly prevalent in various industrial and environmental initiatives.[12,13] According to market analyses recently conducted by the European Bio-plastics Association, it is projected that the global production capacity for bioplastics will experience a substantial increase, rising from 2.11 million tons in 2020 to 2.87 million tons by 2025 with 36% potential growth.[14] Biodegradable plastics, which are manufactured from biobased raw materials such as crops and wood pulp, are intended to be fully decomposed into carbon dioxide, water, and biomass through biological activity in specific mediums (water, soil, and compost), eventually integrating into the natural carbon cycle.[15,16] These plastics, used in products such as packaging, single-use items, and textiles, can come into direct contact with humans.[17]

During use, plastic products inevitably undergo photoaging, which leads to the decomposition and fragmentation of surface

molecules. This process creates conditions conducive to the generation and release of MNPs.[18−20] These particles are predominantly introduced into the human body via gastro-intestinal ingestion,[9] as evidenced by their detection in food, and even human feces,[21] which suggests an interaction with the digestive system. An intake of approximately 39−52 thousand microplastics (MPs) per person annually has been estimated, highlighting significant exposure.[22] Recently, there has been growing interest in understanding MNPs release from plastics, particularly biodegradable plastics, within gastrointestinal environments and examining the associated biological effects.[23,24] Furthermore, compared with traditional plastics, biodegradable plastics are usually more susceptible to environ-mental factors and release more MNPs, resulting in comparable or even more significant toxic effects.[25,26] However, a notable gap remains in the literature regarding the release of MNPs from photoaged biodegradable plastics under gastrointestinal conditions and the related toxicological implications.

In this study, the UV aging behavior and potential photoaging mechanisms of biodegradable PLA/PBAT films, a multifunctional biodegradable plastic,[27] were investigated. The effects of UV aging and simulated gastrointestinal conditions on the mass loss of the films and the underlying factors were subsequently examined. In addition, the impact of MNPs released from UV-aged films under simulated gastro-intestinal conditions on the viability of the THP-1 cell model was elucidated and compared with that of conventional MNPs. This research enhances our understanding of the photoaging of biodegradable plastics and their potential biological risks when exposed to gastrointestinal environments.

■ MATERIALS AND METHODS

Photoaging Experiments

Before starting the aging experiment, the PLA/PBAT films were thoroughly cleaned with ultrapure water to remove surface impurities and then dried at 50 °C. Subsequently, the film underwent artificial aging using a 15 W UV lamp with a 254 nm wavelength at four different simulated UV exposure durations: 0, 5, 10, and 15 d. The aged samples were stored in dark conditions until further experimentation. Although UVA and UVB dominate natural UV aging, UVC (100−280 nm) has been used in artificial accelerated UV aging experiments.[28−30] Additionally, in industrial and public settings, UVC is commonly used for air disinfection and material sterilization, including plastics,[31,32] which may inadvertently contribute to UV-induced aging of plastic products.

Simulated Gastrointestinal Digestion of Films and Collection of MNPs

The plastic films were prepared by cutting them into squares of 5 × 5 mm for the purpose of *in vitro* gastrointestinal simulation digestion, following the method described by Marcos et al.,[33] with minor modifications, including the addition of shaking to simulate gastrointestinal peristalsis and adjustments to the digestion time.[34] Initially, 50 mg of plastic film was suspended in 10 mL of a sterile salt solution (140 mmol/L NaCl, 5 mmol/L KCl), with the pH adjusted to 2.0 using 0.1 mol/L HCl. Following this, 0.5 mL of sterile pepsin solution (25 mg/mL in 0.01 mol/L HCl) was added to the mixture. The resulting suspension was then incubated at 300 rpm in a water bath maintained at 37 °C for a duration of 2 h. Subsequently, the pH of the suspension was altered to 5.5 using 0.1 mol/L NaHCO$_3$ solution, before 0.5 mL of sterile pancreatic bile solution (1.40 mg/mL trypsin and 8 mg/mL bile salts) was added. The pH was further adjusted to approximately 7.0 with the 0.1 mol/L NaHCO$_3$ solution. The total volume was then adjusted to 15 mL using a sterile salt solution (140 mmol/L NaCl, 5 mmol/L KCl, pH 7.0), and the

suspension was incubated again at 300 rpm in a water bath at 37 °C for 5 h. After completing the simulated gastrointestinal digestion, the MNPs were collected by centrifugation at 10,000 rpm for 10 min. To remove any remaining enzymes and salts, the MNPs were sequentially washed twice with 2% SDS and ultrapure water, then freeze-dried and stored away from light. Additionally, ultrafiltration was also used for MNPs collection, with a 300 kDa ultrafiltration tube to capture the released MNPs. The collected MNPs were similarly washed twice with 2% SDS and ultrapure water to remove any remaining enzymes and salts, then resuspended in ultrapure water, freeze-dried, and stored away from light. The films underwent the same washing steps for subsequent characterization. The mass loss ratio of the films and the mass loss was normalized to the film surface area were calculated.

Instrumental Characterization

Macroscopic color change during film aging was captured using a mobile phone camera. The surface morphology, roughness, and fluctuation of the films were characterized by laser confocal microscopy (CLSM, LSM900). The surface microregion morphology of the films was characterized using atomic force microscopy (AFM, JPK Nanowizard 4XP). Infrared spectra of the film surface were acquired using attenuated total reflection Fourier transform infrared spectroscopy (ATR-FTIR, iS50). The morphology and corresponding phase maps of the film surface were characterized using atomic force microscope infrared spectroscopy (AFM-IR, NanoIR3-S), with the infrared spectrum collected in the wavenumber ranges of 940 cm^{-1} to 1220 and 1310 cm^{-1} to 1900 cm^{-1}. Data within the range of 1220 cm^{-1} to 1310 cm^{-1} was missing due to hardware limitations. The laser configuration did not cover this wavelength range, resulting in a lack of signal in this part of the spectrum. Additionally, AFM-IR was employed to analyze MNPs released from the film, with the infrared spectrum gathered in the same wavenumber ranges for both tracer and composition analysis of these MNPs. To avoid interference from hybrid peaks, such as Si−O peaks from a silicon substrate, the MNPs were deposited on a ZnS substrate for the infrared spectrum collection. The aggregation of MNPs was characterized by an optical microscope (Axio Scope 5). The solid film was placed in a high-purity EPR tube and subjected to *in situ* photo irradiation at room temperature for electron paramagnetic resonance (EPR, A200) testing. Additionally, 100 mmol/L DMPO aqueous solution was used to capture potential radical species originating from the film, and the entire process was carried out during the photoaging period. Contact angle measurement was conducted using a contact angle measuring instrument (Dataphysics/OCA50). The surface energy was calculated from the contact angle measurements of different liquids on target surfaces using the Owens−Wendt technique.[35] Ultrapure water and ethylene glycol were used as test liquids. The surface tensions and their components of these liquids were referenced in Prydatko et al.[36] The ζ-potential and hydrodynamic diameter of the MNPs were measured using a Zetasizer (Nano ZS90) at a stable temperature of 25 °C after sufficient ultrasonic dispersion.

Cell Culture

THP-1 cells were procured from Procell Life Science & Technology Co., Ltd. and were cultured under controlled conditions at 37 °C with 5% CO$_2$ and maintained at an optimal humidity level. The culture medium employed was RPMI-1640 (Gibco), supplemented with 10% heat-inactivated FBS (Gibco), 1% penicillin-streptomycin (Gibco), and 2 μL β-mercaptoethanol (aladdin). Prior to commencing each experimental procedure, the cells were meticulously counted and resuspended in an appropriate volume of culture medium to achieve the desired cell density.

Cytotoxicity Assays

The mass of the collected MNPs was measured, and they were resuspended to a specific concentration for subsequent experiments. Cell Counting Kit-8 (CCK-8, Beyotime) was utilized to detect changes in cell viability. Initially, THP-1 cells were cultured with 100 ng/mL phorbol 12-myristate 13-acetate (PMA) in 96-well plates at a density of 5 × 10^4 cells per well for 48 h and differentiated into M0 macrophages. Subsequently, the cells were washed twice with PBS
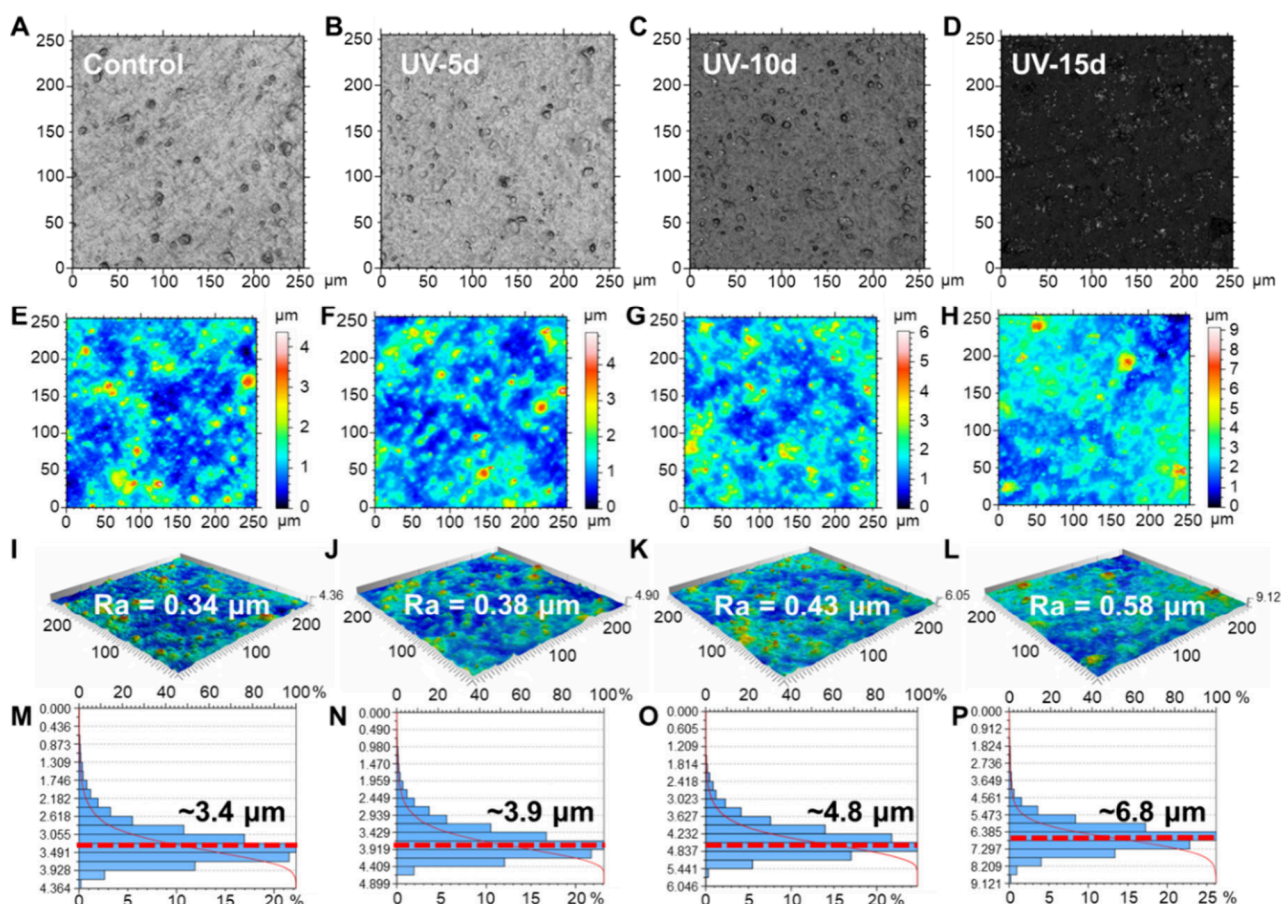
Figure 1. Prolonged UV exposure intensifies the photoaging of PLA/PBAT films. Optical images of the film subjected to ultraviolet light aging over periods of 0, 5, 10, and 15 d (A−D). Two-dimensional (2D, E−H) and corresponding three-dimensional (3D, I−L) CLSM images of the films at these intervals, respectively; a color bar indicates the height mapping, and surface roughness (Ra, Roughness Average) is detailed on each 3D map. Histograms of the frequency distribution of surface height fluctuations after 0, 5, 10, and 15 d of ultraviolet aging (M−P); the red dashed line marks the center of the distribution.

buffer solution. Various concentrations of MNPs (0, 0.1, 1, 10, 100, 200, 500, and 1000 mg/L; final volume: 100 μL) were then introduced to each well and incubated for 24 h, with three replicates for each concentration. Following incubation and cleaning of the culture medium, 10 μL of CCK-8 solution were added to each well, and they were incubated in a cell incubator for another 1 h. Absorbance at 450 nm was then measured using a microplate reader (TECAN, Infinite 200 PRO). Cell viability (%) is expressed as the percentage of absorbance in the experimental group versus the control group. The 4-parameter logistic regression (4-PL) method[37] was employed to fit the curves, and the half-effect concentration EC_{50} of the impacts of MNPs on cell viability were calculated. The equation describing the 4-PL model is as follows:

$$Y = D + \frac{(A - D)}{\left(1 + \left(\frac{x}{C}\right)^{B}\right)}$$

In which Y is the response, D is the response at infinite analyte concentration, A is the response at zero analyte concentration, x is the analyte concentration, C is the inflection point on the calibration curve (EC_{50}), and B is a slope factor.

Statistical Analysis

The data were analyzed with Python (version 3.11.8) and are expressed as the mean ± standard deviation (SD). The data were analyzed by Welch t test, t test, and one-way analysis of variance (ANOVA). Tukey's multiple comparison test was used for further comparisons between groups. A p-value of less than 0.05 was

considered indicative of statistical significance. The actual p-value for the nonsignificant and significant results are shown in Table S4.

■ RESULTS AND DISCUSSION

Photoaging and Physicochemical Characterization of PLA/PBAT Films

The films were exposed to a UV_{254} lamp for durations of 5, 10, and 15 d. The results showed that the films progressively adopted a yellow hue as the aging period increased (Figure S1). This color change is likely due to alterations in the surface chemical states, functional groups, and the films' light absorbance or scattering properties.[38]

To accurately evaluate the effect of photoaging on the surface morphology and roughness of the films, the surface was analyzed using a laser confocal microscope with a characterization range of 250 × 250 μm. By selecting a large area for examination, the test error caused by the uneven distribution of plastic microregions was minimized. The analysis revealed that photoaging resulted in increased debris accumulation on the surface of the plastic films (Figure 1A−D) and a significant increase in surface roughness (Ra), which rose from 0.34 μm before aging to 0.58 μm after 15 d of photoaging, representing an approximate 71% increase (Figure 1E−L). Furthermore, photoaging had a notable effect on the surface fluctuation of the films, which gradually increased with the duration of photoaging (Figure 1M-P). In the control group, the
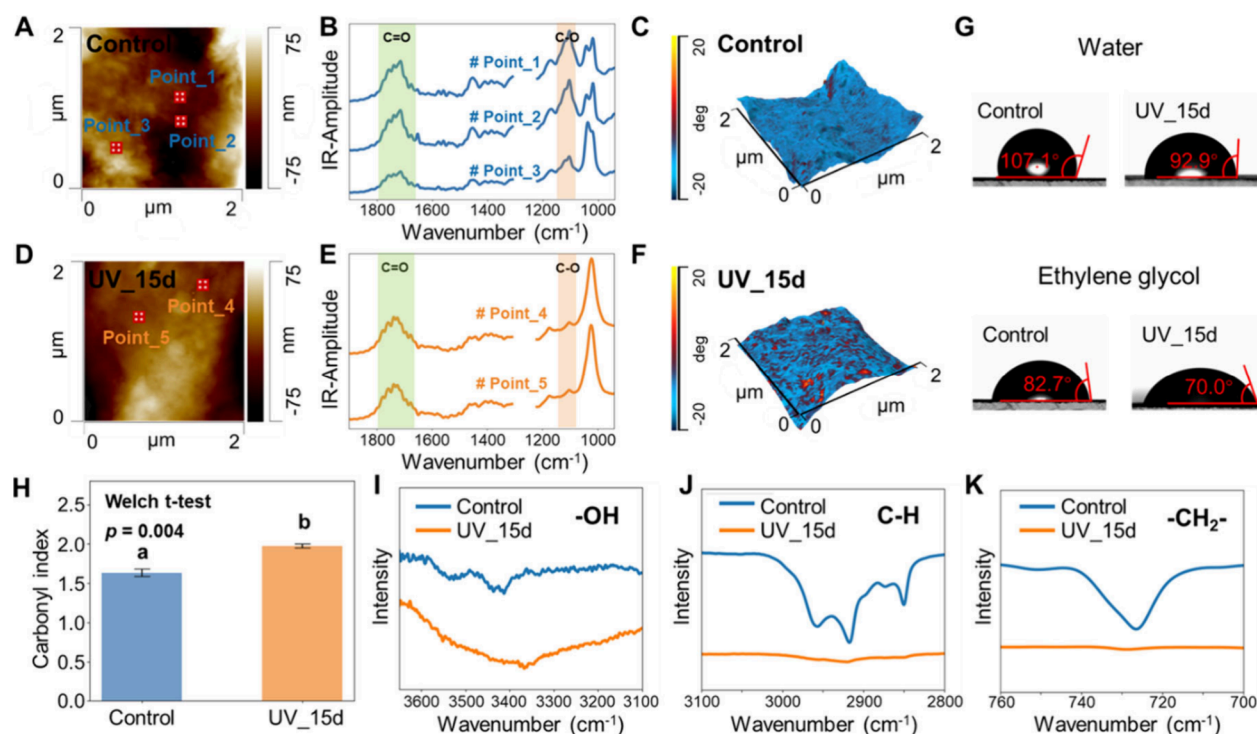
Figure 2. Effect of photoaging on the physicochemical properties of the PLA/PBAT film surface. AFM-IR topography (A), nano infrared spectra of the surface microregion (B), and phase map on 3D topography (C) of the unaged film. AFM-IR topography (D), nano infrared spectra of the surface microregion (E), and phase map on 3D topography (F) of the film after 15 d of ultraviolet aging. Contact angles of the films in water and ethylene glycol before and after photoaging, with surface energy calculated using the Owens−Wendt model (G). Changes in the carbonyl index (CI) before and after photoaging calculated based on nano infrared data (H); The corresponding numeric data are provided in Table S2. Characterization of hydroxyl groups (I) and C−H bonds (J, K) before and after photoaging of the films based on ATR-FTIR. Full ATR-FTIR spectra can be found in Figure S3. Corresponding peak matches are detailed in Table S1.

fluctuation range of the film surface was between 0 and 4.4 μm, with a center at around 3.4 μm. After 15 d of photoaging, however, the fluctuation range expanded significantly to 0 to 9.1 μm, with the center shifting to approximately 6.8 μm. These results suggest that photoaging leads to cracking of the plastic film surface, which facilitates the formation of MNPs that adhere to the surface. This phenomenon was further confirmed by AFM analysis of smaller microregions (Figure S2). Previous studies have commonly used a UV accelerated aging period of within 30 d for biodegradable plastics.[29,39] In our research, it was observed that 15 d of photoaging resulted in the most significant changes on the surface of the plastic films. Based on these findings and the relevant literature, plastic films aged for 15 d were selected for further experiments.

To investigate the effect of photoaging on the chemical functional groups on the surface of plastic films, infrared spectroscopy was performed on films before and after 15 d of photoaging. The characteristic band (Table S1) from 3100 to 3600 cm^{-1} is attributed to −OH stretching vibrations; the range from 2800 to 3100 cm^{-1} is characterized by C−H bond; the band near 1710 cm^{-1} corresponds to C=O stretching vibrations; and the band near 1103 cm^{-1} to C−O left−right symmetric stretching vibration absorption. The bands near 1016 cm^{-1} represent the bending vibration absorption at the surface of adjacent hydrogen atoms on the benzene rings, and the band near 725 cm^{-1} corresponds to the −CH$_2$− groups of PBAT.[29]

The changes in the surface microregions of the films before and after UV aging were characterized using AFM-IR. Two or

three selected points (Figure 2A, D) were analyzed for their infrared spectra (wavelength range: 940 cm^{-1} to 1220 cm^{-1}; 1310 cm^{-1} to 1900 cm^{-1}). Three main peaks were detected at about 1715 cm^{-1}, 1105 cm^{-1}, and 1020 cm^{-1}, corresponding to C=O stretching vibrations, C−O left−right symmetric stretching vibration absorption, and bending vibration absorption at the surface of adjacent hydrogen atoms on the benzene rings, respectively (Figure 2B, E). Significant spectral changes were observed after photoaging, indicating that photoaging can significantly alter the functional groups on the surface of plastic films. The changes in the phase distribution of the film after aging also reflect the chemical changes on the film surface (Figure 2C, F).

Photoaging enhances the hydrophilicity and surface energy of the film, increasing it from 20.76 to 23.20 mN/m (Figure 2G), likely due to an increase in oxygen-containing functional groups on the film surface induced by photoaging. The carbonyl index (CI) is a widely used metric to quantify the degree of aging in polymers, with photoaging typically leading to an increase in the CI.[18] This index is calculated by the ratio of the peak intensity of the carbonyl (C=O) group to that of the methylene (−CH$_2$) group.[18] According to AFM-IR test results, the CI of the film after 15 d of photoaging showed a significant increase, rising from 1.63 to 1.98 (Figure 2H, p = 0.004), an approximate increase of 26%, indicating an increase in the degree of oxidation of the film surface. This trend is consistent with observations by Chang et al.,[40] but contrary to the trends observed by Wang et al.[29] This discrepancy could possibly be explained by the transformation of C=O to C−O
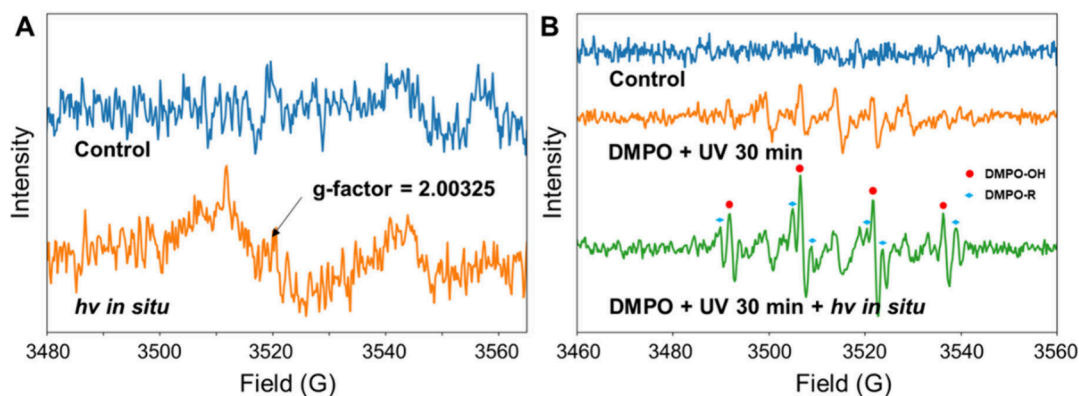
Figure 3. EPR spectra of solid films under *in situ* light exposure (A). EPR spectra were recorded for the DMPO aqueous solution containing MNPs cut from the film under three conditions: unaged (control), after 30 min of UV aging, and after 30 min of UV aging followed by continued *in situ* light exposure (B).
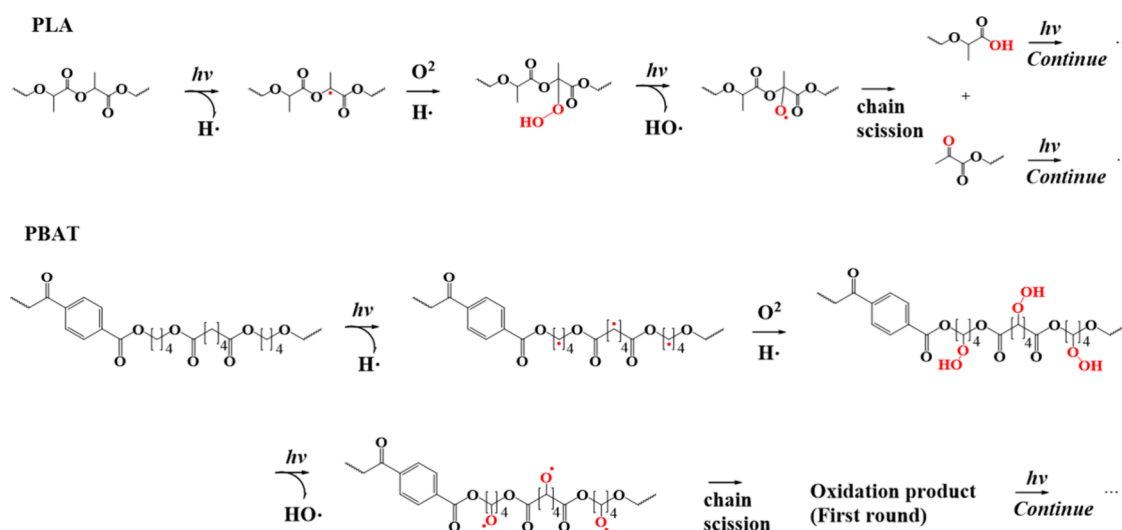
**Figure 4.** Possible photoaging steps of PLA/PBAT film.

or the direct cleavage of the C=O bond during hydrolysis or photoaging, leading to a reduction in the CI index.[29]

Additionally, the changes in peaks of other important functional groups in different wavelength ranges were characterized using ATR-FTIR. An increase in hydroxyl functional groups ($3100-3600$ cm^{-1}) was detected after aging (Figure 2I). Furthermore, the intensity of C−H bonds significantly decreased to nearly complete disappearance after photoaging (Figure 2J, K), consistent with previous observations.[29] This phenomenon may be explained by the following factors: UV exposure can lead to significant photoaging to a depth of about 10 μm on the plastic film's surface,[20] whereas ATR-FTIR, with a detection depth of within 2 μm,[41] is limited to analyzing only the surface layer affected by photoaging. Typically, under UV irradiation, the −CH bonds in the polymer's long chains are broken by the high energy of UV light or react with oxygen in the environment to form oxygen-containing functional groups.[29,42]

The photoaging of plastics is typically accompanied by the generation of free radicals.[38,42,43] EPR was used to test the radical species generated during the photoaging process. Under *in situ* photoaging, the solid film exhibited an EPR signal with a g-factor value of 2.00325 (Figure 3A), indicating that photoaging induces the formation of carbon- and oxygen-centered radicals on the film's surface.[43] The use of DMPO as

a radical spin trap further confirmed the generation of carbon-centered radicals (Figure 3B). Additionally, a significant increase in the peak intensity of hydroxyl radicals was observed with the introduction of continuous *in situ* photoaging (Figure 3B). Previous studies have shown that the photoaging of PLA plastics occurs through Norrish-type photolytic cleavage, specifically involving Norrish Type II reactions.[17]

Based on the above data, Figure 4 illustrates the possible photoaging pathways of PLA/PBAT films, which primarily include the generation of carbon- and oxygen-centered free radicals, chain scission, and the formation of oxidation products of oxygen-containing functional groups, including hydroxyl and carbonyl groups. In the PLA segment of the PLA/PBAT composite films, C−H bond cleavage is likely to occur first at tertiary C−H bonds, as these possess lower bond energy and are more susceptible to light-induced cleavage.[44] The cleavage of tertiary C−H bonds induces the formation of tertiary alkyl radicals. Carbon-centered radicals are highly reactive, readily reacting with atmospheric oxygen to form tertiary peroxy radicals, which subsequently undergo hydrogen abstraction to produce unstable and highly photolabile hydroperoxide groups (ROOH).[42] Our data indicate the presence of oxygen-centered and hydroxyl radicals (Figure 3), speculating the following possible pathway: (ROOH → RO• + HO•). This result is consistent with previous studies, which
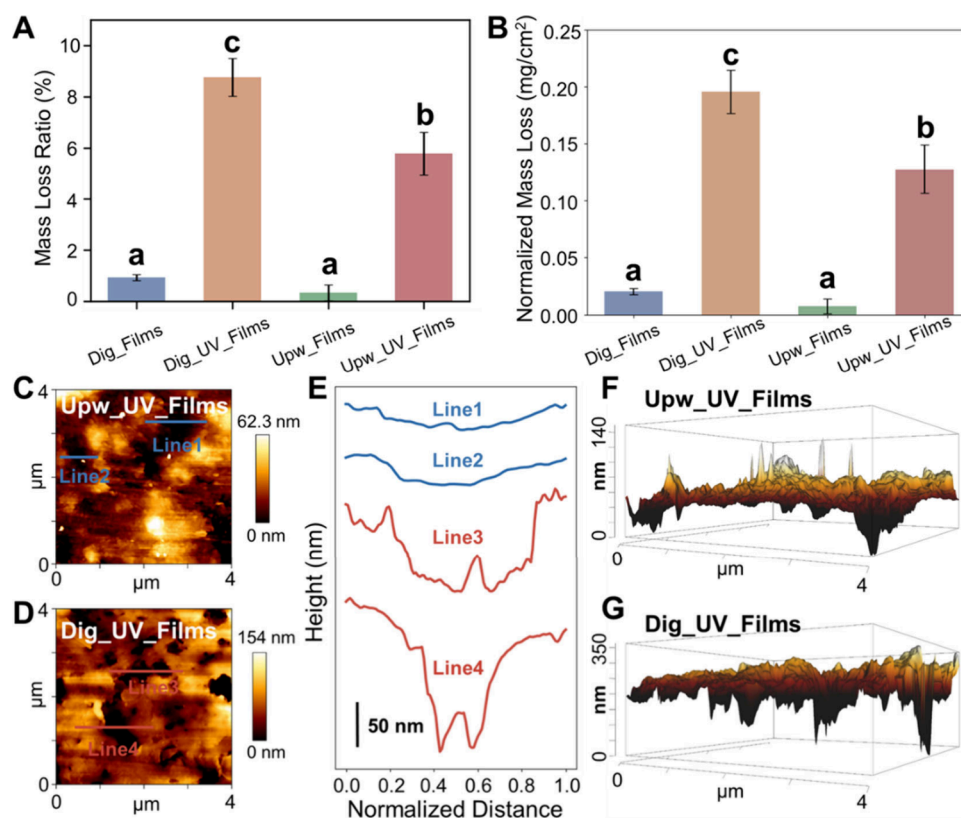
Figure 5. Gastrointestinal digestion promotes mass loss of photoaged films. Comparative mass loss ratio in water and simulated gastrointestinal fluid before and after 15 d of UV aging, starting from an initial mass of 50 mg (A), and mass loss of photoaged PLA/PBAT films, normalized to surface area, in the same conditions (B); the corresponding numeric data are provided in Table S3. Data (mean ± SD) with different superscripts above (one-way analysis of variance and Tukey's post hoc tests, Table S4) were significantly different. The AFM 2D topography morphologies (C) and corresponding 3D topography morphologies (F), along with a height profile line (E, lines 1−2) of the aged film after exposure to water. AFM 2D topography morphologies (D) and corresponding 3D topography morphologies (G), with a height profile line (E, lines 3−4), of the aged film after exposure to simulated gastrointestinal digestive fluid.

suggest that, based on the bond dissociation energies, the dissociation energy of the CO−OH bond is lower than that of C−OOH and COO−H. This indicates that hydroperoxide groups are cleaved to form CO• and •OH, a reaction that predominates under light irradiation,[42] which aligns with the observed increase in the •OH signal during continuous *in situ* photoaging (Figure 3B). In addition, in the PBAT segment of the PLA/PBAT composite films, C−H bond cleavage occurs within the −CH$_2$− groups along the chain (Figure 2K). Due to the similar environment of C−H bonds within −CH$_2$− groups, the initial cleavage theoretically could occur at various positions within the chain.

In Vitro Simulated Gastrointestinal Digestion Promotes Release of MNPs from Photoaged PLA/PBAT Films

Photoaging leads to the formation of MNPs on the film surface, which are likely to be released into the environment. Gastrointestinal intake is considered the primary route through which MNPs enter organisms,[9] making the investigation of plastic behavior in the gastrointestinal environment after photoaging crucial for assessing exposure risks. The gastrointestinal tract presents a unique physiological environment, characterized by the presence of digestive enzymes such as pepsin and trypsin, varying pH levels (stomach: pH ∼ 2; intestines: pH ∼ 7−8), and a variety of ions. These factors can further alter the physicochemical properties of plastics. To investigate the release of MNPs, films that had been photoaged for 15 d were exposed to ultrapure water (Upw) and simulated

gastrointestinal digestive fluids (Dig) *in vitro*. As a control, films that had not undergone photoaging were subjected to the same experimental conditions.

The mass loss ratio of the films, both before and after photoaging, was investigated when exposed to water and *in vitro* simulated gastrointestinal digestive fluids (Figure 5A, Table S3). The results showed that the mass loss ratio of the unaged films was approximately 0.3% in water, likely due to the removal of some unpolymerized plastic fragments from the film surface by water shear forces. The mass loss ratio of the unaged film was only slightly affected by the simulated gastrointestinal digestive fluid, reaching around 0.9%. In contrast, photoaging significantly increased the mass loss ratio, with the ratio rising to about 6% in water and further increasing to approximately 9% in the simulated gastrointestinal fluid (Figure 5A, Table S3, Table S4). Since MNPs are produced and released only from the surface of the film, the mass loss was normalized to the film's surface area. Under water shear forces, the normalized mass loss of aged films reached approximately 0.128 mg/cm^2 (18 times higher than that of unaged films in water). In the gastrointestinal environment, the normalized mass loss further increased to about 0.196 mg/cm^2 (28 times higher). These findings highlight that photoaging is an initiating factor influencing the mass loss of films, with the gastrointestinal digestive environment further exacerbating this loss. Previous studies have shown that lipases in the gut can accelerate the
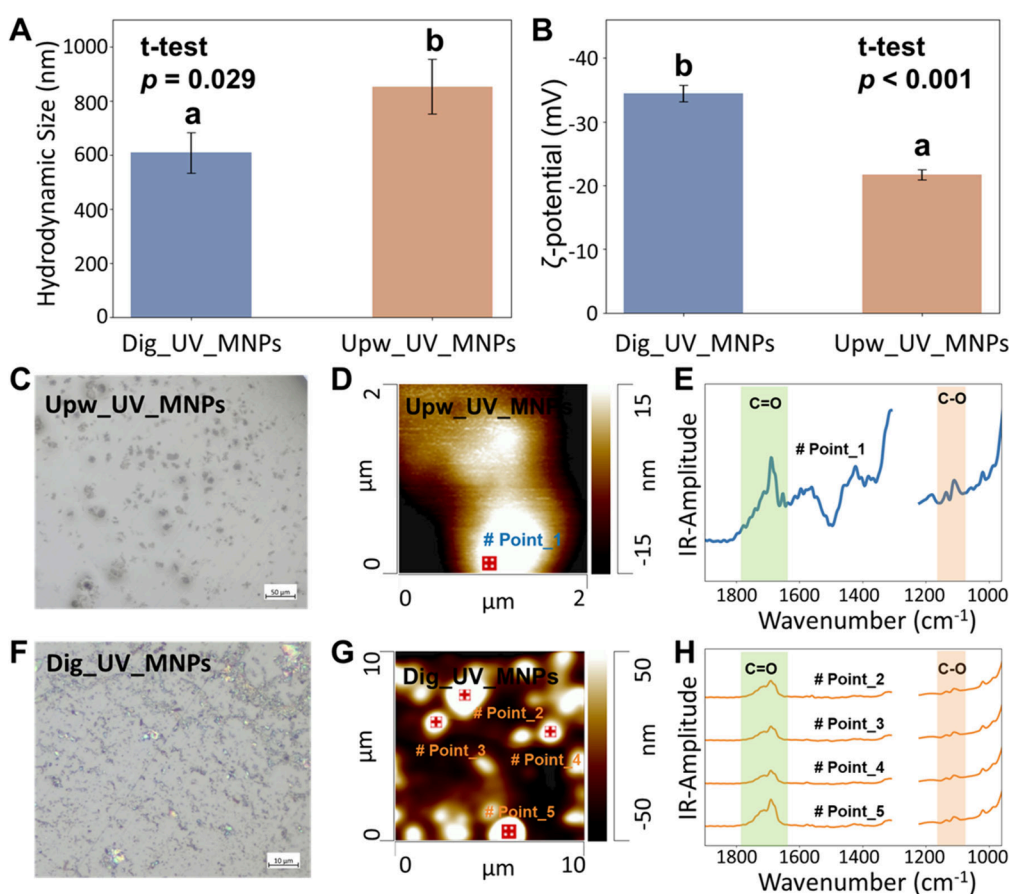
Figure 6. Analysis of MNPs generation and tracing. Hydrodynamic diameter (A) and ζ-potential (B) of MNPs released from photoaged films in water and gastrointestinal environments; The corresponding numeric data are provided in Table S3. Microscopic images of MNPs released from the film after 15 d of aging under the treatment of ultrapure water (C) and simulated gastrointestinal digestive fluid (F). AFM-IR topography (D) and nano infrared spectrum (E) of MNPs released from aged films in water environment. AFM-IR topography (G) and nano infrared spectra (H) of MNPs released from aged films in the simulated gastrointestinal digestion environment. Corresponding peak matches are detailed in Table S1.

degradation of PLA microplastics, leading to the formation of oligomeric nanoparticles.[23] In addition, light also has a positive effect on the swelling-induced fragmentation of the polymer owing to the infiltration of ions.[45] Therefore, the increased mass loss of the photoaged film in the gastrointestinal environment may be related to the enhanced accessibility of digestive enzymes (enzymatic degradation) and ions (swelling effects) on the surface of the aged film, as aging increases the film's hydrophilicity and surface energy (Figure 2G). It is important to note that the *in vitro* gastrointestinal simulated digestion fluid formulation referenced in this study (from Lourdes et al.) does not include lipase. Consequently, in actual gastrointestinal fluids, the mass and quantity of MNPs released from aged PLA/PBAT films may be higher, potentially posing an even greater health risk.

Subsequently, AFM was used to examine the morphology of the aged films after exposure to water and gastrointestinal digestive fluid, respectively. The results revealed that more pores formed on the surface of the photoaged film following exposure to gastrointestinal digestive fluid (Figure 5C, D). These pores were observed to have diameters at the micron or even submicron scale, with depths generally exceeding 100 nm (Figure 5E, red lines, Figure 5G). In contrast, the depth of the pores on the aged film exposed to water typically did not exceed 30 nm (Figure 5E, blue lines, Figure 5F). It is noteworthy that the presence of pores indicates that the release

of MNPs from the aged film in gastrointestinal digestive fluid is uneven. This may be attributed to differences in the phase distribution across the surface of the aging film (Figure 2C, F). AFM phase imaging measures energy dissipation during tip–sample interactions, providing insight into differences in the material's mechanical properties, such as elasticity, viscoelasticity, and adhesive properties.[46] The digestive enzymes and ions in the gastrointestinal digestive fluid likely exhibit a greater affinity for the altered phases of the film's surface, which leads to the uneven release of MNPs and the formation of pores.

The mass loss of the films results in the release of MNPs. MNPs were collected by centrifugation and subjected to ultrasonic dispersion for no more than 5 min before measuring their hydrodynamic size. Prolonged ultrasonic treatment could cause further fragmentation of the MNPs, while without ultrasonic dispersion, MNPs aggregation could adversely affect measurement accuracy, necessitating a compromise between these two factors. During the 5 min ultrasonic dispersion, no significant reduction ($p < 0.05$) in the particle size of model PSMPs was observed (Figure S4), suggesting that size reduction due to ultrasonic dispersion within 5 min is negligible. The hydrodynamic diameters of the dispersed film-derived MNPs were 853 nm in water and 608 nm in gastrointestinal conditions, respectively (Figure 6A, Table S3). Additionally, the ζ-potentials of the film-derived MNPs were
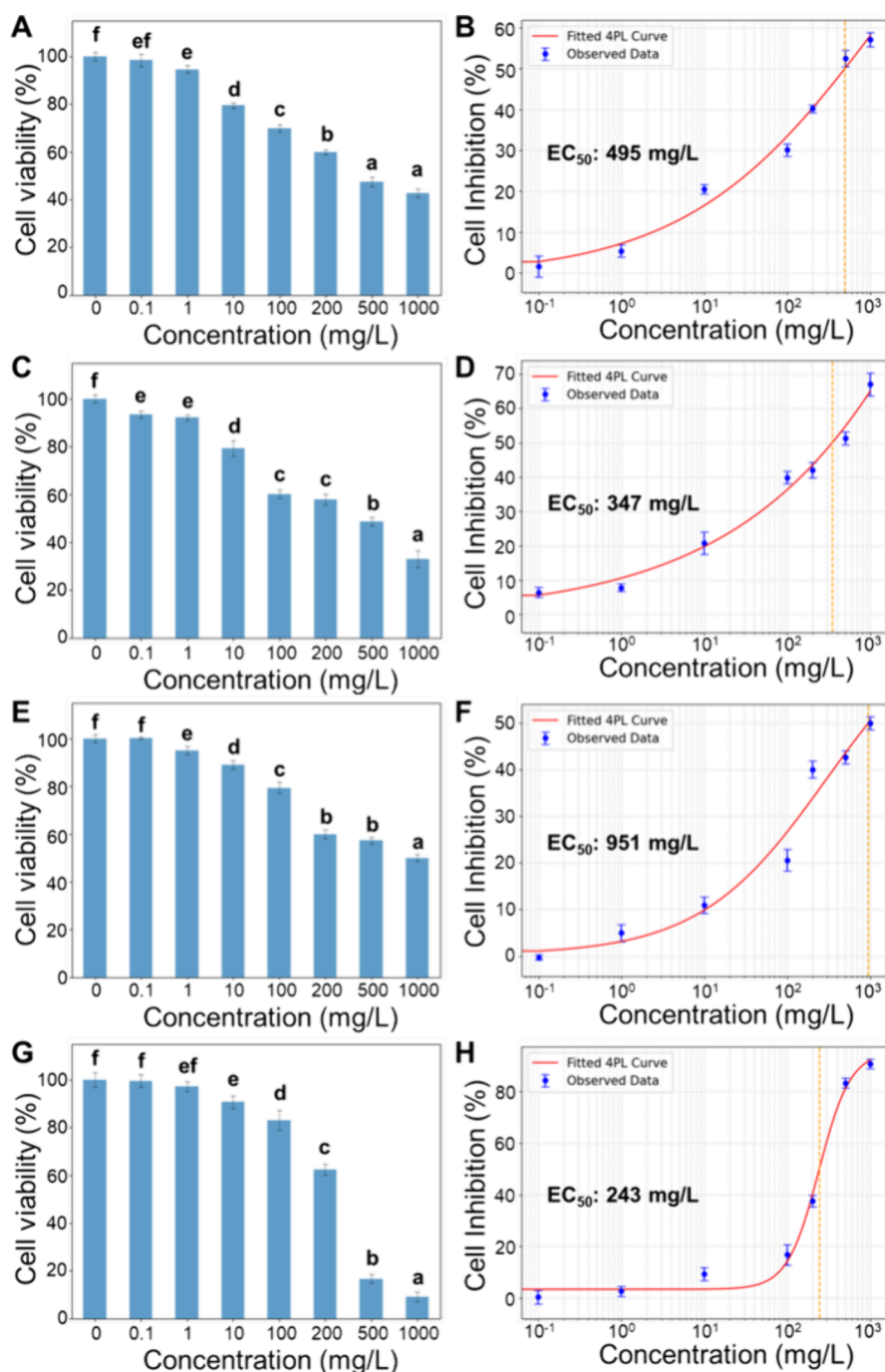
Figure 7. Effects of MNPs on THP-1 cytotoxicity. Cell viability after 24 h exposure to different concentrations of MNPs collected by centrifugation from aged films in the gastrointestinal environment (A) and corresponding 4-PL fitted curves and calculated EC_{50} (B). Cell viability after 24 h exposure to different concentrations of commercialized PS MNPs (C) and corresponding 4-PL fitted curves and calculated EC_{50} (D). Cell viability after 24 h exposure to different concentrations of commercialized PMMA MNPs (E) and corresponding 4-PL fitted curves and calculated EC_{50} (F). Cell viability after 24 h exposure to different concentrations of MNPs collected by ultrafiltration from aged films in the gastrointestinal environment (G) and corresponding 4-PL fitted curves and calculated EC_{50} (H). The corresponding numeric data are provided in Table S3. Data (mean ± SD) with different superscripts above (one-way analysis of variance and Tukey's post hoc tests, Table S4) significantly different.

−21.67 mV in water and −34.4 mV in gastrointestinal simulated digestive fluid. The smaller hydrodynamic particle size and increased negativity of the MNPs in the gastrointestinal environment are likely due to further particle fragmentation and the release of more negatively charged terminal groups, resulting from enzymatic degradation and ion-swelling effect compared to the water environment.

The released MNPs appeared in flake, spherical, and ellipsoidal shapes (Figure 6C, D, F, G). MNPs isolated from the water environment tended to aggregate after drying, resulting in a significantly larger particle size (Figure 6C). This aggregation is likely due to the smaller negative charge on the MNPs released in water (ζ-potential = −21.67 mV), compared to those released in gastrointestinal digestive fluid (ζ-potential = −34.40 mV). The reduced electrostatic repulsion led to

particle agglomeration during the drying process, thereby increasing particle size and limiting the collection of AFM-IR data over a larger test range (Figure 6D).

To further investigate the origin and composition of the released MNPs, nanoscale infrared spectroscopy was conducted on the particles (Figure 6D, G; band range: 940 to 1220 cm^{-1}, and 1310 to 1900 cm^{-1}). The results revealed that three key peaks, similar to those observed on the aged film, were detected (Figure 6E, H; Table S1). These peaks were located at 1690 cm^{-1}, 1110 cm^{-1}, and 1020 cm^{-1}, corresponding to C = O stretching vibration, C−O symmetric stretching vibration, and bending vibration absorption due to adjacent hydrogen atoms on the benzene rings, respectively. The peak at 1020 cm^{-1} was notably weaker, which may indicate that the released MNPs are predominantly composed of PLA. Furthermore, the slight shifts in peak positions (Table S1) are likely due to variations in laser settings and hardware configurations during the measurement process.[47] Interestingly, the CI of MNPs released from the photoaged films in the simulated gastrointestinal environment was significantly increased (Table S2). This rise in CI is likely attributed to the formation of smaller MNPs, which expose more carbonyl groups on their surfaces, resulting in an enhanced CI.

Cytotoxicity of MNPs

Although the mass loss ratio of aged films in the simulated gastrointestinal environment can reach approximately 9% (Figure 5A), it is important to note that this mass loss does not directly correspond to the mass of MNPs collected. This discrepancy arises because the film's mass loss may not be solely attributable to MNPs release but could also include the release of additives, monomers, and other impurities present in the plastic,[48,49] or the direct conversion of plastic carbon into dissolved organic carbon (DOC) under light exposure.[2] Additionally, a certain amount of loss occurs during the MNPs collection process. Consequently, calculating the cytotoxicity of MNPs based solely on film mass loss is likely to underestimate their actual cytotoxic effects. In this context, centrifugation and ultrafiltration methods were employed to collect MNPs. Overall, the ultrafiltration method collected more than twice the mass of MNPs (Figure S5). Moreover, the hydrodynamic size distribution of MNPs collected via ultrafiltration covered a broader range, from tens of nanometers to about 1 μm (Figure S6). Compared to centrifugation, ultrafiltration captured a greater number (over 90%) of smaller-sized MNPs, ranging from tens of nanometers to 300 nm (Figures S6, S7). These findings indicate that ultrafiltration is more effective for collecting smaller MNPs, which are likely lost during the centrifugation collection process.

MNPs have been increasingly detected in various human body fluids and organs, indicating their ability to translocate across biological barriers, enter the circulatory system, and ultimately accumulate in organs and tissues.[50] Therefore, investigating the cytotoxicity of MNPs is essential for assessing their toxicological risks and offers valuable insights into potential health impacts. THP-1 cells were chosen as a model for cytotoxicity testing due to their extensive use in studies on cellular uptake and toxicity, including research on engineered nanoparticles and plastic MNPs.[11,51] Furthermore, as components of the innate immune system, macrophages serve as sentinels that recognize, engulf, and degrade foreign pathogens and particles, including MNPs.[52−54] Cytotoxicity was selected as an initial indicator of cellular stress and

damage, as it represents a crucial end point for evaluating the biological impact of nanoparticles.[55]

First, MNPs collected by centrifugation from aged films in simulated gastrointestinal digestive fluid were exposed to THP-1 cells at various concentrations (0 to 1000 mg/L). The viability of THP-1 cells gradually declined with increasing MNPs concentrations, dropping to 43% at 1000 mg/L (Figure 7A, Table S3). The EC$_{50}$ value was determined to be 495 mg/L (Figure 7B). Then, ultrafiltration was employed to obtain a more comprehensive understanding of the cytotoxicity of the released MNPs. At MNPs concentrations of 500 mg/L and 1000 mg/L collected via ultrafiltration, cell viability further decreased to approximately 16.7% and 9.2%, respectively (Figure 7G, Table S3), with an EC$_{50}$ of around 243 mg/L (Figure 7H). Microscopic images revealed that MNPs collected through ultrafiltration caused more severe cell lysis at high concentrations (Figures S8, S9). These findings indicate that smaller-sized MNPs contribute more significantly to toxic effects in THP-1 macrophages. Smaller plastic particles possess a higher proportion of surface-exposed molecules, enhancing surface reactivity.[4] Additionally, reduced particle size may alter cellular uptake mechanisms, leading to increased internalization, potential membrane damage, and elevated ROS levels.[11,56] Collectively, these factors likely contribute to the observed increase in cell cytotoxic effects.

To further investigate the cytotoxicity of MNPs derived from PLA/PBAT biodegradable films, cell viability tests were conducted using two conventional plastics, polystyrene (PS) and poly(methyl methacrylate) (PMMA), both frequently employed in cytotoxicity studies as representative traditional plastics.[57] The conventional PS and PMMA MNPs exhibited a hydrodynamic particle size distribution similar to that of MNPs collected by centrifugation (Figures S10, S11, S7). Both PS and PMMA MNPs caused a concentration-dependent reduction in THP-1 cell viability (Figure 7C, E). The EC$_{50}$ for PS MNPs was determined to be 347 mg/L (Figure 7D), while the EC$_{50}$ for PMMA was 951 mg/L (Figure 7F). Additionally, PS induced significant cell lysis at high concentrations compared to PMMA (Figures S12, S13). The toxicity of PLA/PBAT-derived MNPs collected by centrifugation on THP-1 cells was observed to be intermediate between that of PS and PMMA. In contrast, MNPs collected by ultrafiltration exhibited the lowest EC$_{50}$. This preliminary comparative analysis suggests that PLA/PBAT-derived MNPs pose a toxicity risk comparable to or even greater than that of conventional plastic MNPs, underscoring the need for comprehensive risk assessments and further research on the health impacts of biodegradable plastics. The EC$_{50}$ values observed in this study are representative as they reflect the potential toxicity of PLA/PBAT-derived MNPs under realistic environmental conditions (gastrointestinal exposure following photoaging), which closely simulate natural exposure scenarios.

■ CONCLUSION AND FUTURE PERSPECTIVE

The study demonstrates that UV-induced aging significantly modifies the physicochemical properties of PLA/PBAT films. Aging caused the films to yellow, increased their hydrophilicity and surface energy, and progressively increased surface roughness and fluctuation in a time-dependent manner. Spherical and flake-like particles emerged in microregions of the film, suggesting polymer chain breakage. Additionally, UV aging led to C−H bond cleavage and an increase in the carbonyl index. The possible photoaging pathways include the

generation of carbon- and oxygen-centered free radicals, chain scission, and the formation of oxidation products of oxygen-containing functional groups including hydroxyl and carbonyl groups. Water shear forces resulted in significant mass loss in aged films in water environments, reaching approximately 0.128 mg/cm^2. In gastrointestinal environments, this mass loss escalated to around 0.196 mg/cm^2, likely due to enzymatic digestion and ion-swelling effects. The increase in mass loss in gastrointestinal environments was reflected by the formation of additional and deeper pores (exceeding 100 nm) on the film surface. This mass loss resulted in the production of MNPs, which were smaller than 1 μm and negatively charged. Nanoinfrared analysis confirmed that these MNPs originated from the aged films and consisted mostly of PLA. Ultra-filtration more effectively collected MNPs released from aged films in gastrointestinal environments, displaying a broader size distribution, particularly of smaller-sized MNPs, and induced a more pronounced toxic effect on THP-1 cells, with an EC$_{50}$ of 243 mg/L. This finding indicates that smaller MNPs contribute more significantly to THP-1 cytotoxicity. Comparative preliminary analysis suggests that PLA/PBAT-derived MNPs may pose toxicity risks comparable to, or greater than, conventional plastic MNPs, including those from PS and PMMA. These findings indicate that UV-aged PLA/PBAT plastics could present exposure risks to organisms in natural environments, particularly when ingested through the gastro-intestinal tract.

Previous studies have shown that nanoplastics are capable of traversing the intestinal barrier, entering the circulatory system, and dispersing across various organ tissues, thereby posing potential health risks.[10] Notably, upon entry into the circulatory system, nanoparticles may acquire a protein corona on their surfaces, which can substantially influence their biological effects and tissue distribution *in vivo*.[58] In light of these findings, it is essential to identify and analyze the composition of the protein corona on the surface of these released MNPs and to assess how this composition impacts the physiological responses of cells to MNPs and their distribution within biological tissues in future research.

◾ ASSOCIATED CONTENT

ⓢ Supporting Information

The Supporting Information is available free of charge at https://pubs.acs.org/doi/10.1021/envhealth.4c00209.

> Materials and chemicals, film color change, AFM microscopic morphology, full ATR-FTIR spectra, MNPs effects on cell morphology, hydrodynamic particle size distribution, infrared spectrum peak assignments, carbonyl index calculations, raw data (mean and standard deviation), statistical significance analysis (PDF)

◾ AUTHOR INFORMATION

Corresponding Authors

Feng Tan − *Key Laboratory of Industrial Ecology and Environmental Engineering (MOE), School of Environmental Science and Technology, Dalian University of Technology, Dalian 116024, China;* ⓘ orcid.org/0000-0003-3806-6198; Email: tanf@dlut.edu.cn

Rui Cai − *Instrumental Analysis Center, Dalian University of Technology, Dalian 116024, China;* Email: cairui@dlut.edu.cn

Authors

Xuri Wu − *Key Laboratory of Industrial Ecology and Environmental Engineering (MOE), School of Environmental Science and Technology, Dalian University of Technology, Dalian 116024, China*

Han Zhang − *Key Laboratory of Industrial Ecology and Environmental Engineering (MOE), School of Environmental Science and Technology, Dalian University of Technology, Dalian 116024, China*

Jingwen Chen − *Key Laboratory of Industrial Ecology and Environmental Engineering (MOE), School of Environmental Science and Technology, Dalian University of Technology, Dalian 116024, China;* ⓘ orcid.org/0000-0002-5756-3336

Yan Wang − *Key Laboratory of Industrial Ecology and Environmental Engineering (MOE), School of Environmental Science and Technology, Dalian University of Technology, Dalian 116024, China;* ⓘ orcid.org/0000-0003-0899-7899

Complete contact information is available at:
https://pubs.acs.org/10.1021/envhealth.4c00209

Notes

The authors declare no competing financial interest.

◾ REFERENCES

(1) Kumar, R.; Verma, A.; Shome, A.; Sinha, R.; Sinha, S.; Jha, P. K.; Kumar, R.; Kumar, P.; Shubham; Das, S.; et al. Impacts of Plastic Pollution on Ecosystem Services, Sustainable Development Goals, and Need to Focus on Circular Economy and Policy Interventions. *Sustainability* **2021**, *13*, 9963.

(2) Tuttle, E.; Wiman, C.; Munoz, S.; Law, K. L.; Stubbins, A. Sunlight-Driven Photochemical Removal of Polypropylene Micro-plastics from Surface Waters Follows Linear Kinetics and Does Not Result in Fragmentation. *Environ. Sci. Technol.* **2024**, *58*, 5461−5471.

(3) Huang, W.; Xia, X. H. Element cycling with micro(nano)plastics. *Science* **2024**, *385* (6712), 933−935.

(4) Gigault, J.; El Hadri, H.; Nguyen, B.; Grassl, B.; Rowenczyk, L.; Tufenkji, N.; Feng, S.; Wiesner, M. Nanoplastics are neither microplastics nor engineered nanoparticles. *Nat. Nanotechnol.* **2021**, *16* (5), 501−507.

(5) MacLeod, M.; Arp, H. P. H.; Tekman, M. B.; Jahnke, A. The global threat from plastic pollution. *Science* **2021**, *373*, 61−65.

(6) Wang, Z. Q.; Zhang, Y. L.; Kang, S. C.; Yang, L.; Shi, H. H.; Tripathee, L.; Gao, T. G. Research progresses of microplastic pollution in freshwater systems. *Sci. Total Environ.* **2021**, *795*, 148888.

(7) Campanale, C.; Galafassi, S.; Savino, I.; Massarelli, C.; Ancona, V.; Volta, P.; Uricchio, V. F. Microplastics pollution in the terrestrial environments: Poorly known diffuse sources and implications for plants. *Sci. Total Environ.* **2022**, *805*, 150431.

(8) Perera, K.; Ziajahromi, S.; Bengtson Nash, S.; Manage, P. M.; Leusch, F. D. L. Airborne Microplastics in Indoor and Outdoor Environments of a Developing Country in South Asia: Abundance, Distribution, Morphology, and Possible Sources. *Environ. Sci. Technol.* **2022**, *56*, 16676−16685.

(9) Liu, Z. G.; You, X. Y. Recent progress of microplastic toxicity on human exposure base on *in vitro* and *in vivo* studies. *Sci. Total Environ.* **2023**, *903*, 166766.

(10) Meng, X. M.; Ge, L.; Zhang, J. W.; Xue, J. K.; Gonzalez-Gil, G.; Vrouwenvelder, J. S.; Li, Z. Y. Systemic effects of nanoplastics on multi-organ at the environmentally relevant dose: The insights in

physiological, histological, and oxidative damages. *Sci. Total Environ.* 2023, *892*, 164687.

(11) Banerjee, A.; Shelver, W. L. Micro- and nanoplastic induced cellular toxicity in mammals: A review. *Sci. Total Environ.* 2021, *755* (Pt 2), 142518.

(12) Kabir, E.; Kaur, R.; Lee, J.; Kim, K. H.; Kwon, E. E. Prospects of biopolymer technology as an alternative option for non-degradable plastics and sustainable management of plastic wastes. *J. Clean. Prod.* 2020, *258*, 120536.

(13) Shruti, V. C.; Kutralam-Muniasamy, G. Bioplastics: Missing link in the era of Microplastics. *Sci. Total Environ.* 2019, *697*, 134139.

(14) Nizamuddin, S.; Chen, C. R. Biobased, biodegradable and compostable plastics: chemical nature, biodegradation pathways and environmental strategy. *Environ. Sci. Pollut. Res.* 2024, *31*, 8387−8399.

(15) Altman, R. The myth of historical biobased plastics. *Science* 2021, *373*, 47−49.

(16) Dilkes-Hoffman, L.; Ashworth, P.; Laycock, B.; Pratt, S.; Lant, P. Public attitudes towards bioplastics - knowledge, perception and end-of-life management. *Resources, Conservation & Recycling* 2019, *151*, 104479.

(17) Ainali, N. M.; Kalaronis, D.; Evgenidou, E.; Kyzas, G. Z.; Bobori, D. C.; Kaloyianni, M.; Yang, X.; Bikiaris, D. N.; Lambropoulou, D. A. Do poly(lactic acid) microplastics instigate a threat? A perception for their dynamic towards environmental pollution and toxicity. *Sci. Total Environ.* 2022, *832*, 155014.

(18) Syranidou, E.; Karkanorachaki, K.; Barouta, D.; Papadaki, E.; Moschovas, D.; Avgeropoulos, A.; Kalogerakis, N. Relationship between the Carbonyl Index (CI) and Fragmentation of Polyolefin Plastics during Aging. *Environ. Sci. Technol.* 2023, *57*, 8130−8138.

(19) Huang, W.; Jiang, G.; Xie, L.; Chen, X.; Zhang, R.; Fan, X. Effect of oxygen-containing functional groups on the micromechanical behavior of biodegradable plastics and their formation of microplastics during aging. *J. Hazard. Mater.* 2024, *463*, 132911.

(20) Chen, Q.; Wang, Q.; Zhang, C.; Zhang, J.; Dong, Z.; Xu, Q. Aging simulation of thin-film plastics in different environments to examine the formation of microplastic. *Water Res.* 2021, *202*, 117462.

(21) Yan, Z. H.; Liu, Y. F.; Zhang, T.; Zhang, F. M.; Ren, H. Q.; Zhang, Y. Analysis of Microplastics in Human Feces Reveals a Correlation between Fecal Microplastics and Inflammatory Bowel Disease Status. *Environ. Sci. Technol.* 2022, *56*, 414−421.

(22) Cox, K. D.; Covernton, G. A.; Davies, H. L.; Dower, J. F.; Juanes, F.; Dudas, S. E. Human Consumption of Microplastics. *Environ. Sci. Technol.* 2019, *53*, 7068−7074.

(23) Wang, M. J.; Li, Q. Q.; Shi, C. Z.; Lv, J.; Xu, Y. D.; Yang, J. J.; Chua, S. L.; Jia, L. R.; Chen, H. W.; Liu, Q.; et al. Oligomer nanoparticle release from polylactic acid plastics catalysed by gut enzymes triggers acute inflammation. *Nat. Nanotechnol.* 2023, *18*, 403−411.

(24) Liang, B.; Deng, Y.; Zhong, Y.; Chen, X.; Huang, Y.; Li, Z.; Huang, X.; Yang, X.; Du, J.; Ye, R.; et al. Gastrointestinal Incomplete Degradation Exacerbates Neurotoxic Effects of PLA Microplastics via Oligomer Nanoplastics Formation. *Adv. Sci.* 2024, *11*, No. e2401009.

(25) Liu, X. M.; Ahmad, S.; Ma, J. K.; Wang, D.; Tang, J. C. Comparative study on the toxic effects of secondary nanoplastics from biodegradable and conventional plastics on Streptomyces coelicolor M145. *J. Hazard. Mater.* 2023, *460*, 132343.

(26) Tong, H. Y.; Zhong, X. C.; Duan, Z. H.; Yi, X. L.; Cheng, F. Q.; Xu, W. P.; Yang, X. J. Micro- and nanoplastics released from biodegradable and conventional plastics during degradation: Formation, aging factors, and toxicity. *Sci. Total Environ.* 2022, *833*, 155275.

(27) Aversa, C.; Barletta, M.; Cappiello, G.; Gisario, A. Compatibilization strategies and analysis of morphological features of poly(butylene adipate-co-terephthalate) (PBAT)/poly(lactic acid) PLA blends: A state-of-art review. *Eur. Polym. J.* 2022, *173*, 111304.

(28) Amaro-Ortiz, A.; Yan, B.; D'Orazio, J. A. Ultraviolet radiation, aging and the skin: prevention of damage by topical cAMP manipulation. *Molecules* 2014, *19* (5), 6202−6219.

(29) Wang, Z. G.; Ding, J. N.; Song, X. J.; Zheng, L. X.; Huang, J. C.; Zou, H.; Wang, Z. Y. Aging of poly (lactic acid)/poly (butylene adipate-co-terephthalate) blends under different conditions: Environmental concerns on biodegradable plastic. *Sci. Total Environ.* 2023, *855*, 158921.

(30) Liu, H.; Jiao, Q.; Pan, T.; Liu, W.; Li, S.; Zhu, X.; Zhang, T. Aging behavior of biodegradable polylactic acid microplastics accelerated by UV/H2O2 processes. *Chemosphere* 2023, *337*, 139360.

(31) Eadie, E.; Hiwar, W.; Fletcher, L.; Tidswell, E.; O'Mahoney, P.; Buonanno, M.; Welch, D.; Adamson, C. S.; Brenner, D. J.; Noakes, C.; et al. Far-UVC (222 nm) efficiently inactivates an airborne pathogen in a room-sized chamber. *Sci. Rep.* 2022, *12* (1), 4373.

(32) Epelle, E. I.; Macfarlane, A.; Cusack, M.; Burns, A.; Mackay, W. G.; Rateb, M. E.; Yaseen, M. Application of Ultraviolet-C Radiation and Gaseous Ozone for Microbial Inactivation on Different Materials. *ACS Omega* 2022, *7* (47), 43006−43021.

(33) Vela, L.; Villacorta, A.; Venus, T.; Estrela-Lopis, I.; Pastor, S.; García-Rodriguez, A.; Rubio, L.; Marcos, R.; Hernández, A. The potential effects of *in vitro* digestion on the physicochemical and biological characteristics of polystyrene nanoplastics. *Environ. Pollut.* 2023, *329*, 121656.

(34) Liu, P.; Wu, X.; Liu, H.; Wang, H.; Lu, K.; Gao, S. Desorption of pharmaceuticals from pristine and aged polystyrene microplastics under simulated gastrointestinal conditions. *J. Hazard. Mater.* 2020, *392*, 122346.

(35) Owens, D. K.; Wendt, R. C. Estimation of the surface free energy of polymers. *J. Appl. Polym. Sci.* 1969, *13*, 1741−1747.

(36) Prydatko, A. V.; Belyaeva, L. A.; Jiang, L.; Lima, L. M. C.; Schneider, G. F. Contact angle measurement of free-standing square-millimeter single-layer graphene. *Nat. Commun.* 2018, *9*, 4185.

(37) Findlay, J. W. A.; Dillard, R. F. Appropriate Calibration Curve Fitting in Ligand Binding Assays. *AAPS Journal* 2007, *9*, E260−E267.

(38) Li, Y.; Liu, Y.; Liu, S. D.; Zhang, L. L.; Shao, H.; Wang, X. J.; Zhang, W. Photoaging of Baby Bottle-Derived Polyethersulfone and Polyphenylsulfone Microplastics and the Resulting Bisphenol S Release. *Environ. Sci. Technol.* 2022, *56*, 3033−3044.

(39) Xie, J.; Yan, Y.; Fan, S.; Min, X.; Wang, L.; You, X.; Jia, X.; Waterhouse, G. I. N.; Wang, J.; Xu, J. Prediction Model of Photodegradation for PBAT/PLA Mulch Films: Strategy to Fast Evaluate Service Life. *Environ. Sci. Technol.* 2022, *56* (12), 9041−9051.

(40) Chang, Q.; Zhu, D. H.; Hu, L. L.; Kim, H.; Liu, Y. N.; Cai, L. Rapid photo aging of commercial conventional and biodegradable plastic bags. *Sci. Total Environ.* 2022, *822*, 153235.

(41) Jiang, Y.; Yi, S.; Wu, P. Y. Application of ATR-FTIR Spectroscopy in Polymer Film Study. *Progress in Chemistry* 2007, *19* (1), 173−185.

(42) Zhu, K.; Jia, H.; Zhao, S.; Xia, T.; Guo, X.; Wang, T.; Zhu, L. Formation of Environmentally Persistent Free Radicals on Microplastics under Light Irradiation. *Environ. Sci. Technol.* 2019, *53* (14), 8177−8186.

(43) Yuan, Z. H.; Huang, Q. J.; Wang, Z. Q.; Wang, H.; Luo, J. M.; Zhu, N. W.; Cao, X. D.; Lou, Z. Y. Medium-Low Temperature Conditions Induce the Formation of Environmentally Persistent Free Radicals in Microplastics with Conjugated Aromatic-Ring Structures during Sewage Sludge Pyrolysis. *Environ. Sci. Technol.* 2022, *56*, 16209−16220.

(44) Tedder, J. M. Which Factors Determine the Reactivity and Regioselectivity of Free Radical Substitution and Addition Reactions? *Angew. Chem., Int. Ed.* 1982, *21* (6), 401−410.

(45) Lai, Y. J.; Dong, L. J.; Sheng, X. Y.; Li, Q. C.; Li, P.; Hao, Z. N.; Yu, S. J.; Liu, J. F. Swelling-Induced Fragmentation and Polymer Leakage of Nanoplastics in Seawater. *Environ. Sci. Technol.* 2022, *56*, 17694−17701.

(46) Wang, D.; Russell, T. P. Advances in Atomic Force Microscopy for Probing Polymer Structure and Properties. *Macromolecules* 2018, *51* (1), 3−24.

(47) Luo, H. W.; Xiang, Y. H.; Zhao, Y. Y.; Li, Y.; Pan, X. L. Nanoscale infrared, thermal and mechanical properties of aged

microplastics revealed by an atomic force microscopy coupled with infrared spectroscopy (AFM-IR) technique. *Sci. Total Environ.* **2020**, *744*, 140944.

(48) Luo, H. W.; Liu, C. Y.; He, D. Q.; Sun, J. Q.; Li, J.; Pan, X. L. Effects of aging on environmental behavior of plastic additives: Migration, leaching, and ecotoxicity. *Sci. Total Environ.* **2022**, *849*, 157951.

(49) Wiesinger, H.; Wang, Z. Y.; Hellweg, S. Deep Dive into Plastic Monomers, Additives, and Processing Aids. *Environ. Sci. Technol.* **2021**, *55*, 9339−9351.

(50) Feng, Y. D.; Tu, C.; Li, R. J.; Wu, D.; Yang, J.; Xia, Y. K.; Peijnenburg, W. J. G. M.; Luo, Y. M. A systematic review of the impacts of exposure to micro- and nano-plastics on human tissue accumulation and health. *EEH* **2023**, *2*, 195−207.

(51) Ge, C. C.; Du, J. F.; Zhao, L. N.; Wang, L. M.; Liu, Y.; Li, D. H.; Yang, Y. L.; Zhou, R. H.; Zhao, Y. L.; Chai, Z. F.; et al. Binding of Blood Proteins to Carbon Nanotubes Reduces Cytotoxicity. *Proc. Natl. Acad. Sci. U.S.A.* **2011**, *108*, 16968−16973.

(52) Chanput, W.; Mes, J. J.; Wichers, H. J. THP-1 cell line: An *in vitro* cell model for immune modulation approach. *Int. Immunopharmacol.* **2014**, *23* (1), 37−45.

(53) Franken, L.; Schiwon, M.; Kurts, C. Macrophages: sentinels and regulators of the immune system. *Cellular Microbiology* **2016**, *18* (4), 475−487.

(54) Brouwer, H.; Porbahaie, M.; Boeren, S.; Busch, M.; Bouwmeester, H. The *in vitro* gastrointestinal digestion-associated protein corona of polystyrene nano- and microplastics increases their uptake by human THP-1-derived macrophages. *Part. Fibre Toxicol.* **2024**, *21* (1), 4.

(55) Puzyn, T.; Rasulev, B.; Gajewicz, A.; Hu, X.; Dasari, T. P.; Michalkova, A.; Hwang, H. M.; Toropov, A.; Leszczynska, D.; Leszczynski, J. Using nano-QSAR to predict the cytotoxicity of metal oxide nanoparticles. *Nat. Nanotechnol.* **2011**, *6* (3), 175−178.

(56) Tavakolpournegari, A.; Annangi, B.; Villacorta, A.; Banaei, G.; Martin, J.; Pastor, S.; Marcos, R.; Hernandez, A. Hazard assessment of different-sized polystyrene nanoplastics in hematopoietic human cell lines. *Chemosphere* **2023**, *325*, 138360.

(57) Weber, A.; Schwiebs, A.; Solhaug, H.; Stenvik, J.; Nilsen, A. M.; Wagner, M.; Relja, B.; Radeke, H. H. Nanoplastics affect the inflammatory cytokine release by primary human monocytes and dendritic cells. *Environ. Int.* **2022**, *163*, 107173.

(58) Monopoli, M. P.; Åberg, C.; Salvati, A.; Dawson, K. A. Biomolecular Coronas Provide the Biological Identity of Nanosized Materials. *Nat. Nanotechnol.* **2012**, *7*, 779−786.